ACS APPLIED NANO MATERIALS

www.acsanm.org Article

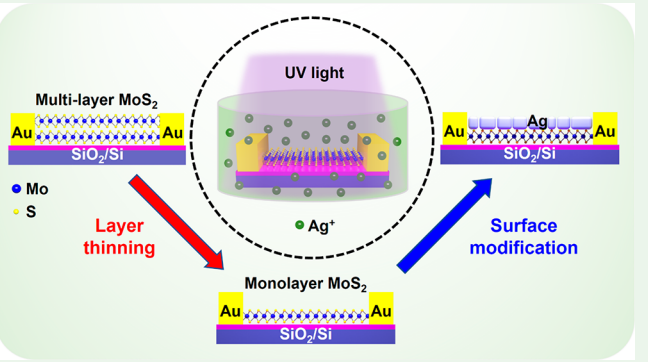
Selective Surface Modification and Layer Thinning of MoS_2 via Ultraviolet-Light Irradiation in an Ionic Solution: Implications for Multifunctional Nanoelectronic Devices

Lei Zhang, Kun Liu, Fanyi Kong, Xue Han, Jianxun Dai, Mengmeng Wang,* Changsen Sun, Huolin Huang, Lujun Pan, and Dawei Li*

Cite This: https://doi.org/10.1021/acsanm.3c00361 Read Online

ACCESS | Metrics & More | Article Recommendations | Supporting Information

ABSTRACT: The electrical properties of transition-metal dichalcogenides (TMDs), such as MoS_2, are highly dependent on carrier doping and layer thickness. The ability to selectively control these two critical characteristics is of great importance in order to develop TMD-based multifunctional nanoelectronic device applications, which remains challenging. Here, we report a strategy for controllable surface modification and layer thinning of MoS_2 via ultraviolet (UV)-light irradiation in a silver ionic (Ag^+) solution environment. The results show that, by adjustment of the UV irradiation time, nanostructured Ag ultrathin films (~2.9 nm) are uniformly deposited on monolayer MoS_2 and can lead to a controllable p-type doping effect, while the thickness of MoS_2 from few-layer to thick-layer could be thinned to the atomic monolayer limit. Both Ag nanostructure deposition and layer thinning have been evidenced to initiate from the edges of MoS_2, independent of the edge type, thus revealing a unique UV-light-assisted defect-induced surface modification and layer-thinning mechanism. Overall, this study provides a simple methodology for the selective control of doping and layer thickness in TMDs, paving the way for developing multifunctional nanoelectronics and integrated optoelectronics.



KEYWORDS: *transition-metal dichalcogenide, surface modification, p-type doping, layer thinning, photoreduction*

INTRODUCTION

Because of their excellent electrical and optoelectronic properties, two-dimensional (2D)-layered materials, such as semiconducting transition-metal dichalcogenides (TMDs), show great potential in diverse device applications,[1−3] including field-effect transistors (FETs),[4−6] photodetectors,[7] nanocavity lasers,[8] optical modulators,[9,10] sensors,[11] and energy storage devices.[12] To realize these applications, it is necessary to control their electrical and optical properties, both of which are highly dependent on the number of layers[13,14] and the surface doping.[15,16] For instance, TMDs from few-layer to bulk materials have indirect band gaps with weak luminescence, while monolayer (1L) TMDs exhibit direct band gaps with strong luminescence[17,18] and also possess other unique properties such as large second-order optical nonlinearities,[19] strong spin-valley coupling,[20] etc. In addition, doping as a simple and most common functionality pathway can not only adjust the band gap but also modulate the conductivity in layered TMDs.[21]

In previous studies, the number of layers (especially the monolayer limit) in TMDs has been controlled via mechanical exfoliation,[22] chemical vapor deposition,[23] plasma etching,[24] and laser thinning.[25,26] On the other hand, several doping techniques have been developed to modulate the inherent properties of TMDs, including chemical doping,[27] single-atom metal doping,[28] laser-assisted doping,[29] and surface modification.[16] However, most of these techniques are complex and limited to only one characteristic control. The ability to control the layer thickness and doping through a single-platform approach is of great importance in order to develop TMD-based multifunctional and integrated device applications, which remains challenging and yet to be demonstrated.

A promising approach to achieve both carrier doping and layer thickness control is the light-assisted post-treatment of layered TMDs.[30,31] In this work, we exploit ultraviolet (UV)-light irradiation to selectively realize surface modification and layer thinning of MoS_2 in a silver ionic (Ag^+) solution (Figure

Received: January 25, 2023
Accepted: March 19, 2023

Downloaded via DALIAN UNIV OF TECHNOLOGY on March 29, 2023 at 03:47:18 (UTC).
See https://pubs.acs.org/sharingguidelines for options on how to legitimately share published articles.

© XXXX American Chemical Society

https://doi.org/10.1021/acsanm.3c00361
ACS Appl. Nano Mater. XXXX, XXX, XXX−XXX

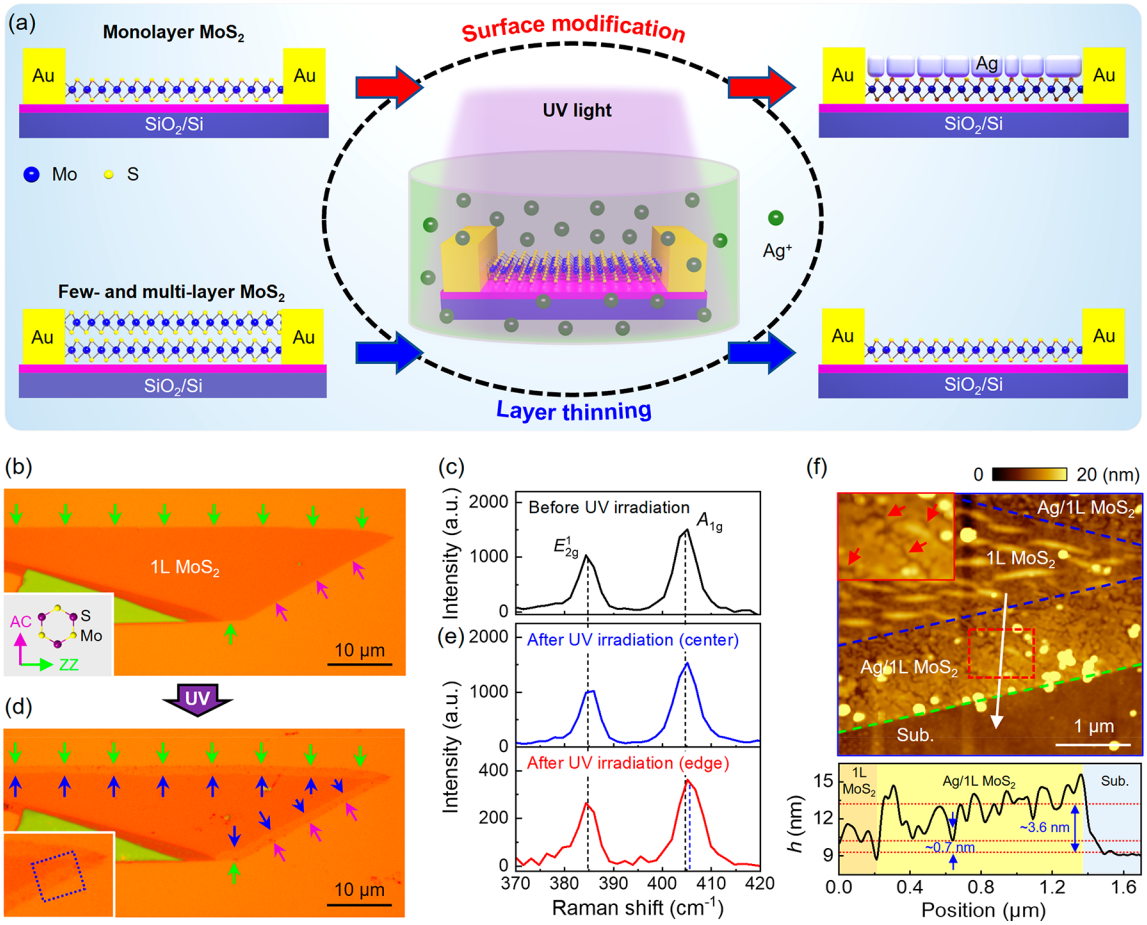


Figure 1. Surface modification in 1L MoS_2. (a) Schematic for selective surface modification and layer thinning of MoS_2 via UV irradiation in a Ag^+ solution. Optical images of a 1L MoS_2 flake (b) before and (d) after UV irradiation in a Ag^+ solution for 20 min. Insets: Crystal orientation of MoS_2 (b) and enlarged optical image of the modified area (d). The green and purple arrows point to the edges of 1L MoS_2; the blue arrows point to the edges of the area modified with Ag nanostructures. (c and e) Raman spectra of the 1L MoS_2 sample shown in parts b and d, respectively. (f) AFM image of the blue dotted square region in the inset of part d, which includes 1L MoS_2, Ag/1L MoS_2, and SiO_2/Si substrate. Bottom inset: Height profile along the white solid line. Top inset: Enlarged AFM image of the red dashed region in part f.

1a). The experimental results show that, under UV-light exposure in a Ag^+ solution environment, nanostructured silver ultrathin films (~2.9 nm) are uniformly decorated on 1L MoS_2 surfaces; meanwhile, the thickness of MoS_2 from few-layer to thick-layer (TL) could be thinned to the atomic monolayer limit. In addition, the as-deposited Ag nanostructures can effectively control the p-type doping in 1L MoS_2 without causing any damage, as evidenced by *in situ* electrical transport, Raman, and photoluminescence (PL) measurements. Moreover, both Ag nanostructure surface modification and layer thinning are observed to start from the edges of MoS_2, revealing a unique UV-light-assisted defect-induced surface modification and thinning mechanism. Therefore, our work offers a simple technique for selectively controlling the doping and layer thickness in TMDs, which can be extended to other van der Waals layered materials.

RESULTS AND DISCUSSION

UV-Light Interaction with 1L MoS_2 in a Ag^+ Solution. We prepare MoS_2 flakes with different layer thicknesses by mechanical exfoliation and then transfer them onto the SiO_2 (285 nm)/Si substrates by a dry transfer technique. Figure 1b show the optical image of a 1L MoS_2 flake, with its layer thickness confirmed by the Raman frequency difference between E^1_{2g} (384.7 cm^{-1}) and A_{1g} (404.7 cm^{-1}) (Figure 1c). We find that the 1L MoS_2 sample in Figure 1b has two edges with an angle of about 30°: one edge is long and straight (green arrows), while the other is relatively short (purple arrows). According to previous studies,[32] the long and short edges correspond to the zigzag (ZZ) and armchair (AC) orientations of MoS_2, respectively (Figure 1b, inset). Next, we immerse the sample in a Ag^+ solution and perform UV-light-irradiation treatment (wavelength = 254 nm; Figure 1a). After exposure with UV light for a fixed time (Figure 1d), an optical contrast change occurs from two edges of 1L MoS_2 (blue arrows), which can be more clearly identified in the inset of Figure 1d. A similar phenomenon has been observed in more 1L MoS_2 samples (Figure S1), indicating that the appearance of an optical contrast change is not limited to the types of MoS_2 edges.

There are two possible reasons for this optical contrast change in 1L MoS_2: surface corrosion or surface modification. To understand this phenomenon, we first perform Raman spectroscopy analysis. The Raman spectra of 1L MoS_2 taken at the edge area (with an optical change) and center area (without an optical change) are similar (Figures 1e and S2), consistent with that before UV irradiation (Figure 1c). In addition, there is no formation of any defect-related Raman

https://doi.org/10.1021/acsanm.3c00361
ACS Appl. Nano Mater. XXXX, XXX, XXX−XXX

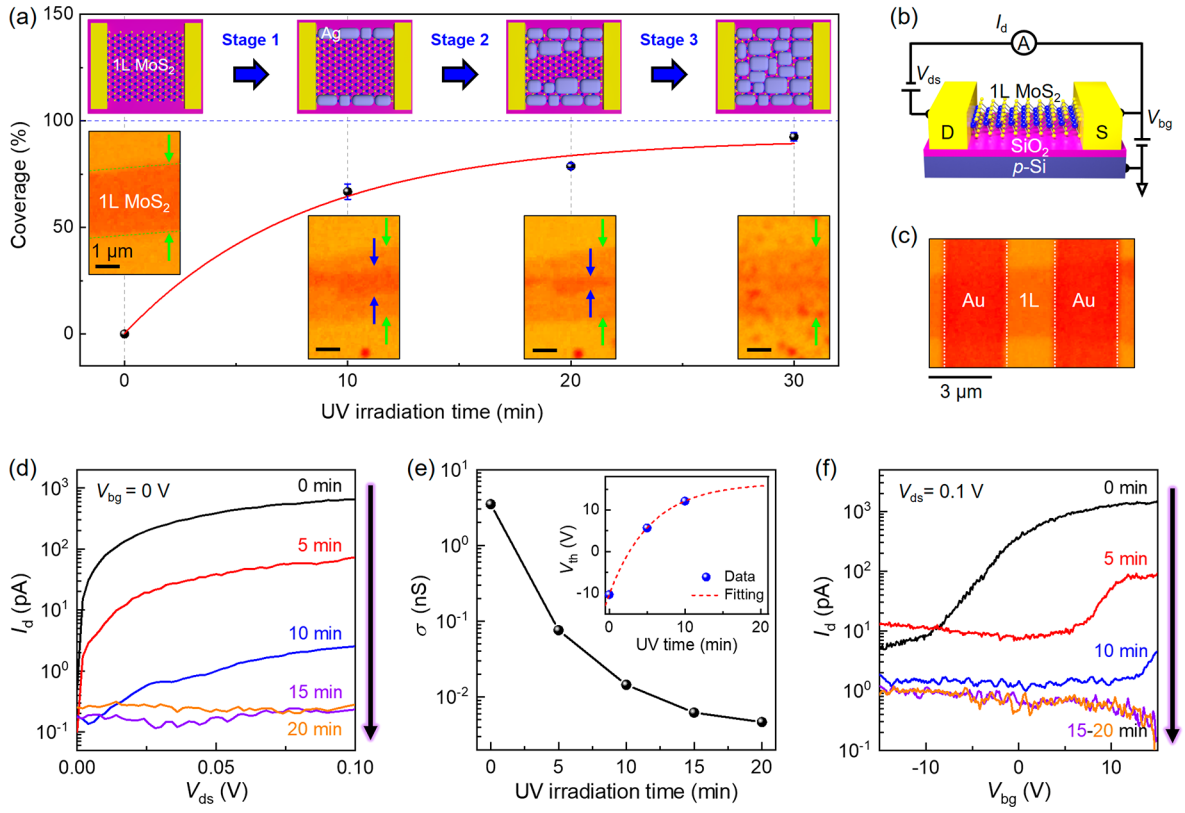


Figure 2. *In situ* optical and electrical monitoring of the surface modification process in 1L MoS_2. (a) Coverage of as-deposited Ag nanostructures on 1L MoS_2 as a function of the UV-irradiation time. The dots and solid line are the experimental data and fitting curve, respectively. Lower insets: Corresponding optical images. The green and blue arrows point to the edges of pristine and reacting 1L MoS_2, respectively. Upper insets: Scheme of the surface modification process in 1L MoS_2. (b) 1L MoS_2 FET device schematic. (c) Optical image of a 1L MoS_2 device, where Au electrodes are indicated by dotted lines. (d) *In situ* I_d versus V_{ds} (V_{bg} = 0 V) characteristics of a 1L MoS_2 device after UV irradiation in a Ag^+ solution for different time. (e) Conductivity σ versus UV-irradiation time. Inset: Threshold V_{th} extracted from part f versus UV-irradiation time. (f) *In situ* I_d versus V_{bg} (V_{ds} = 0.1 V) characteristics of the 1L MoS_2 device after UV irradiation in a Ag^+ solution for different time.

peaks and other possible chemical bonds, such as Ag_2S (~244 cm^{-1}) and Mo−O (~820 cm^{-1}) (Figure S3),[33,34] strongly confirming that the lattice structure of 1L MoS_2 at the edge area (with an optical change) is not damaged. Hence, the possibility of surface corrosion in 1L MoS_2 can be ruled out. Energy-dispersive X-ray (EDX) analyses (Figure S4) reveal that the change in optical contrast is due to surface modification with Ag coatings on 1L MoS_2, as is further evidenced by atomic force microscopy (AFM) studies. Figure 1f shows the AFM image for the blue dotted square in the inset of Figure 1d, which includes three regions: 1L MoS_2, Ag/1L MoS_2, and SiO_2/Si substrate. It is obvious that the Ag/1L MoS_2 region is composed of a discontinuous nanostructured Ag thin film and a 1L MoS_2 underneath. In contrast, very few Ag nanostructures are deposited on the SiO_2/Si substrate. The height difference between the crack in the area of Ag/1L MoS_2 (Figure 1f, top inset) and the substrate is measured to be about 0.7 nm (Figure 1f, bottom inset), which is in good agreement with the thickness of 1L MoS_2. Hence, the film thickness of as-deposited Ag nanostructures can be estimated to be about 2.9 nm.

According to the observation in Figure 1, surface modification with Ag nanostructures prefers to initiate from the edges of 1L MoS_2. As is known, there are more defects at the edge than at the center area.[35] Previous studies have shown that the formation of defects within 1L MoS_2 could introduce active sites, thereby leading to a significant improvement of the catalytic properties.[36] Therefore, in our case, we reasonably propose a UV-light-assisted defect-induced surface modification mechanism in 1L MoS_2. To confirm this speculation, we prepare a 1L MoS_2 flake without edges by a photolithography technique and then perform UV-light treatment in a Ag^+ solution (Figure S5). As expected, there is not any Ag nanostructure deposition and not any change in the lattice structure for this 1L MoS_2 sample.

Next, we quantitively investigate the nanostructured Ag thin-film deposition process on 1L MoS_2. Figure 2a shows different steps of surface modification under UV irradiation, where Ag nanostructures simultaneously nucleate from two edges of MoS_2 (green arrows, Stage 1), then expand and go inward (blue arrows, Stage 2), and finally reach full coverage (Stage 3). We also have calculated the coverage of Ag nanostructures on the surface of MoS_2 using the equation $S_{Ag}/S_{MoS_2} \times 100\%$, where S_{Ag} and S_{MoS_2} are the total areas of Ag nanostructures and pristine MoS_2, respectively. The fitting curve in Figure 2a demonstrates a typical parabola relationship between S_{Ag}/S_{MoS_2} and UV-irradiation time, similar to the photocatalytic behavior of Ag nanostructure deposition on other 2D materials.[37]

To gain a better understanding of the surface modification process and its effect on the electrical properties of MoS_2, we design a FET device in a two-terminal configuration (Figure 2b) and perform *in situ* electrical measurement. Figure 2c shows the optical image of a 1L MoS_2 device on a SiO_2/Si

https://doi.org/10.1021/acsanm.3c00361
ACS Appl. Nano Mater. XXXX, XXX, XXX−XXX

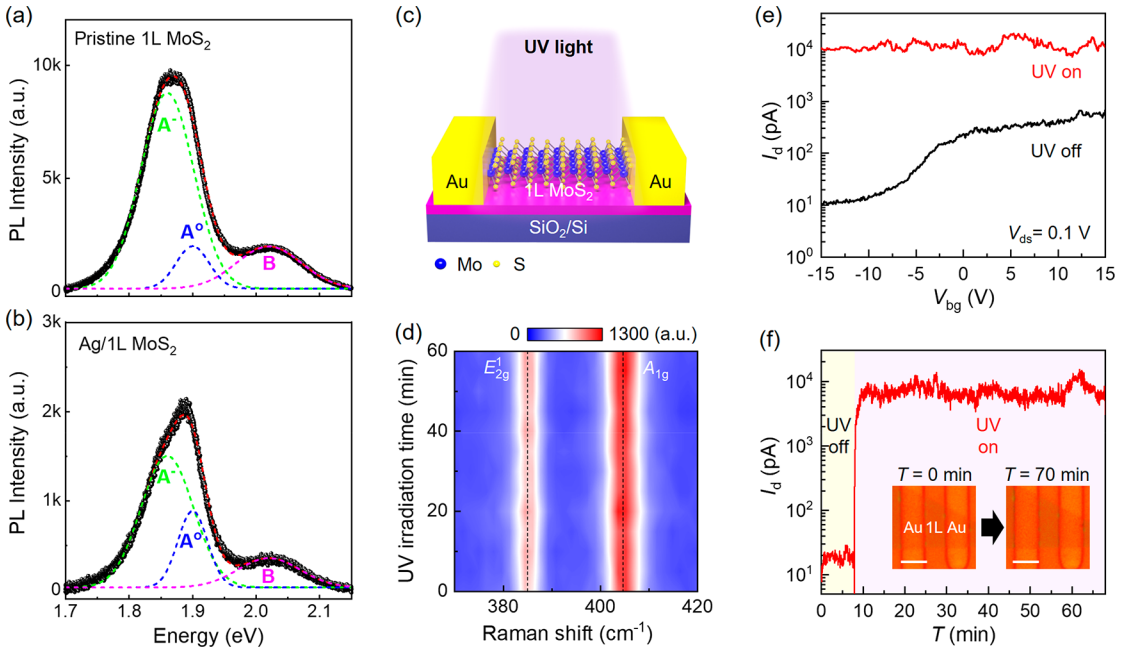


Figure 3. Mechanism for tuning the electrical and optical properties of 1L MoS_2 via UV irradiation in a Ag^+ solution. (a and b) PL spectra for (a) pristine 1L MoS_2 and (b) Ag/1L MoS_2. The PL spectra are well fitted with three excitonic peaks: a negative trion (A^-), a neutral exciton (A^0), and B exciton. (c) Schematic of a 1L MoS_2 device by UV-light treatment in air. (d) Raman spectra of a 1L MoS_2 sample after UV irradiation for different time in air. (e) I_d versus V_{bg} (V_{ds} = 0.1 V) characteristics of a 1L MoS_2 device taken in the dark (black curve) and under UV-light exposure (red curve). (f) I_d versus time (T) relationship (V_{ds} = 0.1 V) for a 1L MoS_2 device (inset). Scale bar: 5 μm.

substrate fabricated by transferring an exfoliated sample on top of two parallel Au electrodes. The channel width and length are about 2 and 3 μm, respectively. Figure 2d compares the drain current (I_d) versus drain-source voltage (V_{ds}) characteristics for 1L MoS_2 in Figure 2c after UV irradiation in a Ag^+ solution for different time. The conductivity (σ) extracted from Figure 2d gradually decreases with an increase in the UV-irradiation time (or S_{Ag}/S_{MoS_2} ratio) (Figure 2e), revealing a controllable carrier (electron or hole) doping in 1L MoS_2 by varying the Ag nanostructure modification. To confirm the doping effect, we perform *in situ* electrical transport measurement (Figure 2f). It can be seen that the pristine 1L MoS_2 FET exhibits a typical n-type semiconducting behavior (Figure S6). After modification with Ag nanostructures, I_d (or σ) is significantly decreased in the whole gating range, representing a heavy hole (or p-type) doping. In addition, Ag nanostructure modification induces a threshold voltage (V_{th}) shift toward the forward gate voltage (V_{bg}) direction (Figure 2e, inset). This is another key indicator of a p-type doping effect in 1L MoS_2.[38]

Optical characterization is also an effective approach to probing the doping effect in 1L TMDs.[39] Parts a and b of Figure 3 analyze the room temperature PL spectra of 1L MoS_2 without and with Ag nanostructure deposition. We quantitatively fit the PL spectra using a Gaussian model with three peaks, associated with a B exciton peak at 2.02 eV, a neutral exciton peak (A^0) at 1.90 eV, and a negative trion peak (A^-) at 1.86 eV. The intensity ratios between A^- and A^0 are 12.2 for 1L MoS_2 and 6.6 for Ag/1L MoS_2, suggesting reduced electron doping in Ag/1L MoS_2. This optical behavior can be explained in that the presence of Ag nanostructures results in the internal electron loss in 1L MoS_2. In addition, Raman spectra of 1L MoS_2 (Figure 1e) show that the A_{1g} peak position blue shifts by ~1 cm^{-1} after the deposition of Ag nanostructures, which further confirms the p-type doping effect.[40]

According to previous reports,[34,41] UV-ozone treatment is capable of inducing structural defects in 1L MoS_2 and then influencing its optical and electrical properties (e.g., reduction of σ). To exclude the possibility of this occurrence in our case, we investigate the structural and optoelectronic properties of 1L MoS_2 by UV-light treatment in an air atmosphere (Figure 3c). Figure 3d shows the UV-irradiation time (t)-dependent Raman spectra for a 1L MoS_2 flake. As t increases, both the peak intensity and width of the E^1_{2g} (and A_{1g}) mode remain stable. Meanwhile, no significant signal change is observed in the time-dependent PL spectra (Figure S7), thereby suggesting no structural defects generated in 1L MoS_2. We then characterize the photoresponse behavior of 1L MoS_2 FET using UV light as the excitation source. As shown in Figure 3e, when irradiated under 254 nm UV light, I_d (or σ) is significantly increased by over 1 order of the magnitude throughout the whole gating range, which could return back to its original state when UV light is turned off. In addition, the current signal remains stable even under UV-light irradiation for a long time (≥70 min; Figure 3f). These experimental results provide strong evidence of neither structural degradation nor property change in 1L MoS_2 via UV irradiation. Hence, modulation of the electrical properties of 1L MoS_2 in Figure 2 is mainly attributed to the surface modification of Ag nanostructures. Overall, UV-light-assisted surface modification could effectively control the S_{Ag}/S_{MoS_2} ratio and then the p-type doping level in 1L MoS_2.

UV-Light Interaction with Few-Layer to TL MoS_2 in a Ag^+ Solution. How about UV-light interaction with few-layer MoS_2 in a Ag^+ solution environment? To answer this question, we mechanically exfoliate a bilayer (2L) MoS_2 flake (together with a 1L flake) on a SiO_2/Si substrate (Figure 4a), and its layer thickness was determined by Raman spectroscopy. After exposure with UV light in a Ag^+ solution for a short time (<5

https://doi.org/10.1021/acsanm.3c00361
ACS Appl. Nano Mater. XXXX, XXX, XXX−XXX

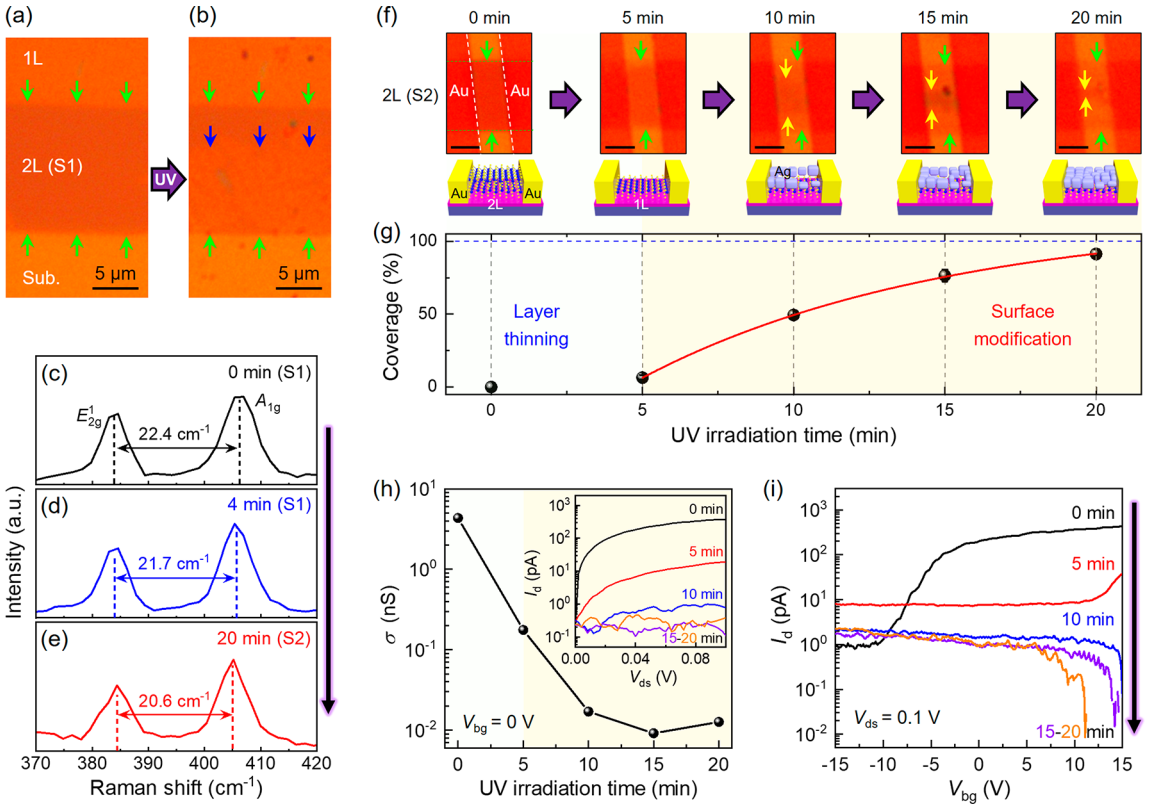


Figure 4. UV-light interaction with 2L MoS_2 in a Ag^+ solution. Optical images of a 2L MoS_2 (S1) flake (a) before and (b) after UV irradiation in a Ag^+ solution for 4 min. The green and blue arrows point to the edges of pristine and reacting 2L MoS_2, respectively. Raman spectra for 2L MoS_2 (c) before and after UV irradiation in a Ag^+ solution for (d) 4 and (e) 20 min. (f–i) *In situ* optical and electrical monitoring of UV-light interaction with a 2L MoS_2 (S2) device in a Ag^+ solution. (f) Optical images of a S2 device after UV irradiation in a Ag^+ solution for different time. The green and yellow arrows point to the edges of pristine 2L MoS_2 and the edges of the Ag/MoS_2 region, respectively. Scale bar: 2 μm. Lower insets: Corresponding device schematics. (g) Coverage (S_{Ag}/S_{MoS_2}) versus UV-irradiation time relationship. The dots and solid line are the experimental data and fitting curve, respectively. (h) σ versus t and I_d versus V_{ds} (inset) characteristics. (i) I_d versus V_{bg} (V_{ds} = 0.1 V) characteristics of a S2 device after UV irradiation in a Ag^+ solution for different time.

min), the optical contrast at most areas of 2L MoS_2 has changed in brightness (Figure 4b), which is close to that of pristine 1L MoS_2. To understand this optical behavior, we perform Raman spectroscopy analysis (Figure 4c–e). It is found that the Raman frequency difference between the E^1_{2g} and A_{1g} modes is changed from 22.4 cm^{-1} (pristine area, Figure 4c) to 21.7 cm^{-1} (reacting area, Figure 4d), strongly confirming that layer thinning of MoS_2 from 2L to 1L occurs.[14]

To investigate the effect of the UV-irradiation time, we fabricate a 2L MoS_2 device and perform *in situ* optical and electrical measurements (Figure 4f–i). Figure 4f shows the optical images of a 2L MoS_2 device after UV irradiation in a Ag^+ solution for different time. In the initial stage ($0 < t \leq 5$ min), the optical contrast of the whole 2L channel becomes bright (similar to Figure 4b), which is attributed to the layer-thinning effect. When $t > 5$ min, the 2L channel exhibits an optical behavior similar to that observed in 1L MoS_2 (Figure 2a), where the optical contrast becomes brighter from two edges of MoS_2 ($t \sim 10$ min), then goes inward ($t \sim 15$ min), and finally realizes a full color change ($t \geq 20$ min). Raman analyses in Figure 4e reveal that 1L MoS_2 formed in the initial stage remains stable even with long-time ($t = 20$ min) UV irradiation in a Ag^+ solution. Hence, we suggest that surface modification with Ag nanostructures is the likely reason for the observed optical contrast change in the later time period. Figure 4g shows the S_{Ag}/S_{MoS_2} versus t curve for a 2L MoS_2 device, which exhibits a parabola relationship when $t > 5$ min, in good agreement with that of 1L MoS_2 (Figure 2a). According to the above analyses, we conclude that selective layer thinning and surface modification could be realized in 2L MoS_2 (Figure 4f, inset). Next, we carry out *in situ* σ versus t (Figure 4h) and electrical transport (Figure 4i) measurements. Both experimental results demonstrate that the electrical properties of 2L MoS_2 are well modulated via layer thinning ($0 < t \leq 5$ min) and surface modification ($5 < t \leq 20$ min), which could be explained by the thickness-dependent electron mobility[42] and the Ag-deposition-induced p-type doping effect,[40] respectively.

To investigate the UV-light interaction with multilayer MoS_2 in a Ag^+ solution, MoS_2 flakes with different thicknesses are exfoliated on a SiO_2/Si substrate. A MoS_2 flake consisted of 1L to 6L, and their respective layer numbers are shown in Figure 5a. The numbers of layers have been precisely verified by combining Raman spectroscopy (Figure 5b)[14] and optical contrast (black curve, Figure 5c).[43] After exposure with UV light in a Ag^+ solution for a relatively long time (~60 min, Figure 5d), MoS_2 flakes with different thicknesses all still exist. More interestingly, the optical contrast of MoS_2 ranging from 2L to 6L has changed into what is comparable to the 1L region (red curve, Figure 5c), which indicates that layer thinning could also be realized in few-layer to multilayer samples. Finally, we have extended our investigation to the TL ones.

https://doi.org/10.1021/acsanm.3c00361
ACS Appl. Nano Mater. XXXX, XXX, XXX−XXX

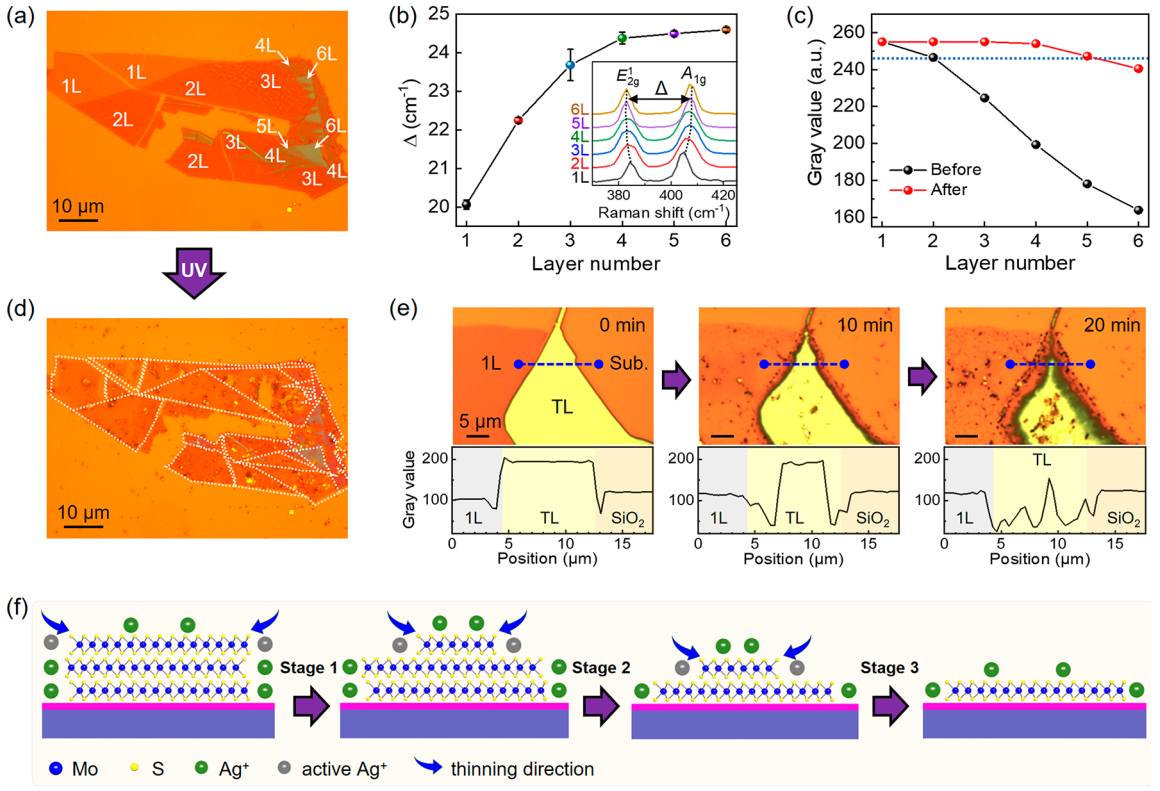


Figure 5. UV-light interaction with multilayer to TL MoS_2 in a Ag^+ solution. Optical images of a MoS_2 flake consisting of 1L to 6L (a) before and (d) after UV irradiation in a Ag^+ solution for 60 min. (b) Raman frequency difference (Δ) as a function of the MoS_2 layer thickness. Inset: Raman spectra for MoS_2 in part a with different layer thicknesses. (c) Gray value extracted from the sample in parts a and d as a function of the layer thickness. The blue dotted line represents 2L MoS_2. (e) Optical images of a TL (~40 nm) MoS_2 under UV irradiation for different time. Lower insets: Corresponding gray-value profiles along the blue dashed lines. (f) Proposed mechanism of layer thinning in MoS_2 via UV irradiation in a Ag^+ solution environment.

Figure 5e compares the optical images of a TL MoS_2 flake with a thickness of ~40 nm after UV irradiation in a Ag^+ solution for different time. As expected, layer thinning occurs in the TL sample. Similar to the surface modification process in 1L MoS_2, layer thinning also starts from the edges of MoS_2 (Figure 5e inset). It is noted that the layer-thinning rate in TL MoS_2 is significantly slower than that in the few-layer one, which can be utilized to fabricate thickness-dependent MoS_2 heterojunction devices.[44]

On the basis of the above analyses, we propose a physical model for a better understanding of the layer thinning and surface modification in MoS_2 via UV irradiation in a Ag^+ solution environment. For simplicity, here we take 3L MoS_2 as an example (Figure 5f). First, the layer thinning (or etching) starts from the edges of the top layer due to its high photocatalytic activity (Stage 1). When the top layer disappears, the second layer is exposed to the Ag^+ solution environment and starts to be etched in the same way (Stage 2). This process is repeated until the layered MoS_2 becomes a monolayer. Finally, Ag nanostructures are photodeposited on the surface of 1L MoS_2 following the process in Figure 2a (Stage 3). This behavior can be well explained by an interface-modified surface potential,[45] where the built-in electric field at the MoS_2/SiO_2 interfaces cannot be completely shielded with decreasing MoS_2 layer numbers. In our case, the unshielded internal electric field originating from the 1L MoS_2/SiO_2 interface can help the surface diffusion of photogenerated carriers and then enhance the photocatalytic activity of 1L MoS_2, thereby leading to Ag nanostructure deposition [$Ag^+ + e^-$ (CB: 1L MoS_2) → Ag] but not etching on 1L MoS_2. However, ≥2L MoS_2 samples have insignificant photocatalytic performances,[45] which thus could be etched via photoreduction to the monolayer limit.[35] We believe that our developed UV-light-assisted selective surface modification and layer-thinning approach could be applicable to many other van der Waals layered materials.

CONCLUSIONS

In summary, we report selective control of the surface modification and layer thickness of MoS_2 via UV-light irradiation in a Ag^+ solution environment. By UV-light treatment in a Ag^+ solution, nanostructured Ag ultrathin (~2.9 nm) films could be uniformly photodeposited on 1L MoS_2, which can induce controllable p-type doping without causing any lattice structural damage. On the other hand, few-layer to TL MoS_2 could be efficiently thinned to the monolayer limit with high crystallinity. On the basis of the *in situ* electrical transport and *in situ* optical spectroscopy analyses, we propose a UV-light-assisted defect-induced surface modification and thinning mechanism. More importantly, the surface modification and layer thinning of MoS_2 can be selectively realized via the proposed single-platform approach, which is simple, convenient, and contactless. Our study thus presents a new strategy for tuning the intrinsic properties of TMDs, which is important for developing 2D material-based nanoelectronic and optoelectronic device applications.

https://doi.org/10.1021/acsanm.3c00361
ACS Appl. Nano Mater. XXXX, XXX, XXX−XXX

METHODS

Sample Preparation. The MoS_2 flakes with different layer thicknesses are mechanically exfoliated from their bulk materials (Six Carbon Technology, China) and then transferred onto the SiO_2 (285 nm)/Si substrates. Their layer thicknesses are identified by combining optical microscopy (ECLIPSE LV150N, Nikon, Japan), Raman spectroscopy (Renishaw inVia), and AFM (MFP-3D, Oxford) measurements. The MoS_2 FET devices are fabricated by the standard photolithography process. Briefly, Au/Ti (10 nm/2 nm) electrodes are prepatterned on the SiO_2/Si substrate, and then MoS_2 flakes on a gel film are transferred to the top of the prepatterned Au/Ti electrodes using a dry transfer technique.[14]

UV-Irradiation Treatment of MoS_2 in a Ag^+ Solution. The MoS_2 samples and FET devices are immersed in a 3 mM $AgNO_3$ solution and then exposed to UV light (wavelength = 254 nm; power density = 18 $\mu W/cm^2$) for a fixed irradiation time (Figure 1a). *In situ* optical and electrical measurements are performed during the UV-light-irradiation process. For comparison, we carry out UV-light treatment and UV photoresponse experiments in an air atmosphere.

Characterizations. The morphologies of MoS_2 and Ag/MoS_2 composites are characterized by an optical microscopy and AFM system. The structure and composition of our samples are analyzed by field-emission scanning electron microscopy (JSM-7900F, JEOL, Japan) with EDX detection capability. The optical properties of MoS_2 samples are investigated by a micro-Raman and PL system. Both Raman and PL signals are collected by focusing a 532 nm laser (power = 1.85 mW) onto the sample surface through a 50× objective. The electrical and photoresponse measurements are carried out using a semiconductor device analyzer (B1500A, Keysight, USA) in combination with a probe station (CM-4, Shenzhen Cindbest Technology Co., Ltd., China).

ASSOCIATED CONTENT

Supporting Information

The Supporting Information is available free of charge at https://pubs.acs.org/doi/10.1021/acsanm.3c00361.

Optical images of a 1L MoS_2 flake, Raman mapping, broadband Raman spectra of 1L MoS_2, EDX spectra for 1L MoS_2 and Ag/1L MoS_2, 1L MoS_2 transistor device characterization, and PL spectra of 1L MoS_2 (PDF)

AUTHOR INFORMATION

Corresponding Authors

Mengmeng Wang − *Laser Micro/Nano Fabrication Laboratory, School of Mechanical Engineering, Beijing Institute of Technology, Beijing 100081, China*; Email: mwang6@bit.edu.cn

Dawei Li − *School of Optoelectronic Engineering and Instrumentation Science, Dalian University of Technology, Dalian 116024, China*; orcid.org/0000-0001-6967-4968; Email: dwli@dlut.edu.cn

Authors

Lei Zhang − *School of Optoelectronic Engineering and Instrumentation Science, Dalian University of Technology, Dalian 116024, China*

Kun Liu − *School of Optoelectronic Engineering and Instrumentation Science, Dalian University of Technology, Dalian 116024, China*

Fanyi Kong − *School of Optoelectronic Engineering and Instrumentation Science, Dalian University of Technology, Dalian 116024, China*

Xue Han − *School of Optoelectronic Engineering and Instrumentation Science, Dalian University of Technology, Dalian 116024, China*

Jianxun Dai − *School of Optoelectronic Engineering and Instrumentation Science, Dalian University of Technology, Dalian 116024, China*

Changsen Sun − *School of Optoelectronic Engineering and Instrumentation Science, Dalian University of Technology, Dalian 116024, China*

Huolin Huang − *School of Optoelectronic Engineering and Instrumentation Science, Dalian University of Technology, Dalian 116024, China*

Lujun Pan − *School of Physics, Dalian University of Technology, Dalian 116024, China*; orcid.org/0000-0003-3666-408X

Complete contact information is available at: https://pubs.acs.org/10.1021/acsanm.3c00361

Notes

The authors declare no competing financial interest.

ACKNOWLEDGMENTS

This work was supported by the National Natural Science Foundation of China (NSFC; Grant 12274051) and the Fundamental Research Funds for the Central Universities [Grants DUT21RC(3)032 and DUT22ZK109]. L.P. acknowledges support from the NSFC (Grants 51972039 and 52272288). H.H. acknowledges support from the Applied Basic Research Project of Liaoning Province, China (Grant 182022JH2/101300259) and the Dalian Science and Technology Innovation Fund, China (Grant 2022JJ12GX011). X.H. acknowledges support from the NSFC (Grant 62105053) and the Fundamental Research Funds for the Central Universities (Grant DUT21LK07).

REFERENCES

(1) Yu, W.; Gong, K.; Li, Y.; Ding, B.; Li, L.; Xu, Y.; Wang, R.; Li, L.; Zhang, G.; Lin, S. Flexible 2D Materials beyond Graphene: Synthesis, Properties, and Applications. *Small* **2022**, *18*, 2105383.

(2) Yan, Z.; Yang, H.; Yang, Z.; Ji, C.; Zhang, G.; Tu, Y.; Du, G.; Cai, S.; Lin, S. Emerging Two-Dimensional Tellurene and Tellurides for Broadband Photodetectors. *Small* **2022**, *18*, 2200016.

(3) Mu, H.; Yu, W.; Yuan, J.; Lin, S.; Zhang, G. Interface and surface engineering of black phosphorus: a review for optoelectronic and photonic applications. *Materials Futures* **2022**, *1*, 012301.

(4) Cui, X.; Lee, G.-H.; Kim, Y. D.; Arefe, G.; Huang, P. Y.; Lee, C.-H.; Chenet, D. A.; Zhang, X.; Wang, L.; Ye, F.; Pizzocchero, F.; Jessen, B. S.; Watanabe, K.; Taniguchi, T.; Muller, D. A.; Low, T.; Kim, P.; Hone, J. Multi-terminal transport measurements of MoS_2 using a van der Waals heterostructure device platform. *Nat. Nanotechnol.* **2015**, *10*, 534−540.

(5) Li, D.; Sun, S.; Xiao, Z.; Song, J.; Shao, D.-F.; Tsymbal, E. Y.; Ducharme, S.; Hong, X. Giant transport anisotropy in ReS_2 revealed via nanoscale conducting-path control. *Phys. Rev. Lett.* **2021**, *127*, 136803.

(6) Li, D.; Sun, S.; Wang, K.; Ahmadi, Z.; Shield, J. E.; Ducharme, S.; Hong, X. Assembly of close-packed ferroelectric polymer nanowires via interface-epitaxy with ReS_2. *Adv. Mater.* **2021**, *33*, 2100214.

(7) Wu, D.; Guo, J.; Wang, C.; Ren, X.; Chen, Y.; Lin, P.; Zeng, L.; Shi, Z.; Li, X. J.; Shan, C.-X.; Jie, J. Ultrabroadband and high-detectivity photodetector based on WS_2/Ge heterojunction through defect engineering and interface passivation. *ACS Nano* **2021**, *15*, 10119−10129.

(8) Wu, S.; Buckley, S.; Schaibley, J. R.; Feng, L.; Yan, J.; Mandrus, D. G.; Hatami, F.; Yao, W.; Vučković, J.; Majumdar, A.; Xu, X. Monolayer semiconductor nanocavity lasers with ultralow thresholds. *Nature* **2015**, *520*, 69−72.

(9) Li, D.; Huang, X.; Xiao, Z.; Chen, H.; Zhang, L.; Hao, Y.; Song, J.; Shao, D.-F.; Tsymbal, E. Y.; Lu, Y.; Hong, X. Polar coupling enabled nonlinear optical filtering at MoS_2/ferroelectric heterointerfaces. *Nat. Commun.* **2020**, *11*, 1422.
(10) Gan, X.; Englund, D.; Van Thourhout, D.; Zhao, J. 2D materials-enabled optical modulators: From visible to terahertz spectral range. *Applied Physics Reviews* **2022**, *9*, 021302.
(11) Dodda, A.; Jayachandran, D.; Pannone, A.; Trainor, N.; Stepanoff, S. P.; Steves, M. A.; Radhakrishnan, S. S.; Bachu, S.; Ordonez, C. W.; Shallenberger, J. R.; Redwing, J. M.; Knappenberger, K. L.; Wolfe, D. E.; Das, S. Active pixel sensor matrix based on monolayer MoS_2 phototransistor array. *Nat. Mater.* **2022**, *21*, 1379.
(12) Gao, J.; Li, L.; Tan, J.; Sun, H.; Li, B.; Idrobo, J. C.; Singh, C. V.; Lu, T.-M.; Koratkar, N. Vertically oriented arrays of ReS_2 nanosheets for electrochemical energy storage and electrocatalysis. *Nano Lett.* **2016**, *16*, 3780−3787.
(13) Mondal, M.; Dash, A. K.; Singh, A. Optical microscope based universal parameter for identifying layer number in two-dimensional materials. *ACS Nano* **2022**, *16*, 14456−14462.
(14) Li, D.; Xiong, W.; Jiang, L.; Xiao, Z.; Rabiee Golgir, H.; Wang, M.; Huang, X.; Zhou, Y.; Lin, Z.; Song, J.; Ducharme, S.; Jiang, L.; Silvain, J.-F.; Lu, Y. Multimodal Nonlinear Optical Imaging of MoS_2 and MoS_2-Based van der Waals Heterostructures. *ACS Nano* **2016**, *10*, 3766−3775.
(15) Chaves, A.; Azadani, J. G.; Alsalman, H.; da Costa, D. R.; Frisenda, R.; Chaves, A. J.; Song, S. H.; Kim, Y. D.; He, D.; Zhou, J.; Castellanos-Gomez, A.; Peeters, F. M.; Liu, Z.; Hinkle, C. L.; Oh, S.-H.; Ye, P. D.; Koester, S. J.; Lee, Y. H.; Avouris, P.; Wang, X.; Low, T. Bandgap engineering of two-dimensional semiconductor materials. *npj 2D Mater. Appl.* **2020**, *4*, 29.
(16) Reed-Lingenfelter, S. N.; Chen, Y.; Yarali, M.; Charboneau, D. J.; Curley, J. B.; Hynek, D. J.; Wang, M.; Williams, N. L.; Hazari, N.; Quek, S. Y.; Cha, J. J. Compact super electron-donor to monolayer MoS_2. *Nano Lett.* **2022**, *22*, 4501−4508.
(17) Mak, K. F.; Lee, C.; Hone, J.; Shan, J.; Heinz, T. F. Atomically thin MoS_2: A new direct-gap semiconductor. *Phys. Rev. Lett.* **2010**, *105*, 136805.
(18) Dandu, M.; Biswas, R.; Das, S.; Kallatt, S.; Chatterjee, S.; Mahajan, M.; Raghunathan, V.; Majumdar, K. Strong single-and two-photon luminescence enhancement by nonradiative energy transfer across layered heterostructure. *ACS Nano* **2019**, *13*, 4795−4803.
(19) Wen, X.; Gong, Z.; Li, D. Nonlinear optics of two-dimensional transition metal dichalcogenides. *InfoMat* **2019**, *1*, 317−337.
(20) Robert, C.; Park, S.; Cadiz, F.; Lombez, L.; Ren, L.; Tornatzky, H.; Rowe, A.; Paget, D.; Sirotti, F.; Yang, M.; et al. Spin/valley pumping of resident electrons in WSe_2 and WS_2 monolayers. *Nat. Commun.* **2021**, *12*, 5455.
(21) Zhang, F.; Lu, Y.; Schulman, D. S.; Zhang, T.; Fujisawa, K.; Lin, Z.; Lei, Y.; Elias, A. L.; Das, S.; Sinnott, S. B.; Terrones, M. Carbon doping of WS_2 monolayers: Bandgap reduction and p-type doping transport. *Sci. Adv.* **2019**, *5*, eaav5003.
(22) Lee, C.; Li, Q.; Kalb, W.; Liu, X.-Z.; Berger, H.; Carpick, R. W.; Hone, J. Frictional characteristics of atomically thin sheets. *Science* **2010**, *328*, 76−80.
(23) You, J.; Hossain, M. D.; Luo, Z. Synthesis of 2D transition metal dichalcogenides by chemical vapor deposition with controlled layer number and morphology. *Nano Convergence* **2018**, *5*, 26.
(24) Liu, Y.; Nan, H.; Wu, X.; Pan, W.; Wang, W.; Bai, J.; Zhao, W.; Sun, L.; Wang, X.; Ni, Z. Layer-by-layer thinning of MoS_2 by plasma. *ACS Nano* **2013**, *7*, 4202−4209.
(25) Castellanos-Gomez, A.; Barkelid, M.; Goossens, A. M.; Calado, V. E.; van der Zant, H. S. J.; Steele, G. A. Laser-thinning of MoS_2: On demand generation of a single-layer semiconductor. *Nano Lett.* **2012**, *12*, 3187−3192.
(26) Wang, M.; Li, D.; Liu, K.; Guo, Q.; Wang, S.; Li, X. Nonlinear optical imaging, precise layer thinning, and phase engineering in $MoTe_2$ with femtosecond laser. *ACS Nano* **2020**, *14*, 11169−11177.
(27) Choi, M. S.; Qu, D.; Lee, D.; Liu, X.; Watanabe, K.; Taniguchi, T.; Yoo, W. J. Lateral MoS_2 p−n junction formed by chemical doping for use in high-performance optoelectronics. *ACS Nano* **2014**, *8*, 9332−9340.
(28) Zhang, J.; Xu, X.; Yang, L.; Cheng, D.; Cao, D. Single-atom Ru doping induced phase transition of MoS_2 and S vacancy for hydrogen evolution reaction. *Small Methods* **2019**, *3*, 1900653.
(29) Rho, Y.; Lee, K.; Wang, L.; Ko, C.; Chen, Y.; Ci, P.; Pei, J.; Zettl, A.; Wu, J.; Grigoropoulos, C. P. A laser-assisted chlorination process for reversible writing of doping patterns in graphene. *Nat. Electron.* **2022**, *5*, 505−510.
(30) Zhang, R.; Xie, Z.; An, C.; Fan, S.; Zhang, Q.; Wu, S.; Xu, L.; Hu, X.; Zhang, D.; Sun, D.; Chen, J.-H.; Liu, J. Ultraviolet light-induced persistent and degenerated doping in MoS_2 for potential photocontrollable electronics applications. *ACS Appl. Mater. Interfaces* **2018**, *10*, 27840−27849.
(31) Kwon, H.; Seo, S. W.; Kim, T. G.; Lee, E. S.; Lanh, P. T.; Yang, S.; Ryu, S.; Kim, J. W. Ultrathin and flat layer black phosphorus fabricated by reactive oxygen and water rinse. *ACS Nano* **2016**, *10*, 8723−8731.
(32) Guo, Y.; Liu, C.; Yin, Q.; Wei, C.; Lin, S.; Hoffman, T. B.; Zhao, Y.; Edgar, J. H.; Chen, Q.; Lau, S. P.; Dai, J.; Yao, H.; Wong, H. S. P.; Chai, Y. Distinctive in-plane cleavage behaviors of two-dimensional layered materials. *ACS Nano* **2016**, *10*, 8980−8988.
(33) Dias, C.; Proenca, M.; Fernandes, L.; Tavares, P.; Vilarinho, R.; Moreira, J. A.; Araújo, J.; Ventura, J. Tuning the stoichiometry of Ag_2S thin films for resistive switching applications. *J. Nanosci. Nanotechnol.* **2016**, *16*, 2608−2612.
(34) Yang, H. I.; Park, S.; Choi, W. Modification of the optoelectronic properties of two-dimensional MoS_2 crystals by ultraviolet-ozone treatment. *Appl. Surf. Sci.* **2018**, *443*, 91−96.
(35) Lei, Y. T.; Li, D. W.; Zhang, T. C.; Huang, X.; Liu, L.; Lu, Y. F. One-step selective formation of silver nanoparticles on atomic layered MoS2 by laser-induced defect engineering and photoreduction. *J. Mater. Chem. C* **2017**, *5*, 8883−8892.
(36) Ye, G.; Gong, Y.; Lin, J.; Li, B.; He, Y.; Pantelides, S. T.; Zhou, W.; Vajtai, R.; Ajayan, P. M. Defects engineered monolayer MoS_2 for improved hydrogen evolution reaction. *Nano Lett.* **2016**, *16*, 1097−1103.
(37) Kong, F.; Zhang, L.; Cong, T.; Wu, Z.; Liu, K.; Sun, C.; Pan, L.; Li, D. Tunable photochemical deposition of silver nanostructures on layered ferroelectric $CuInP_2S_6$. *J. Appl. Phys.* **2022**, *132*, 044103.
(38) Pan, Y.; Wang, X.; Zhang, W.; Tang, L.; Mu, Z.; Liu, C.; Tian, B.; Fei, M.; Sun, Y.; Su, H.; Gao, L.; Wang, P.; Duan, X.; Ma, J.; Ding, M. Boosting the performance of single-atom catalysts via external electric field polarization. *Nat. Commun.* **2022**, *13*, 3063.
(39) Mouri, S.; Miyauchi, Y.; Matsuda, K. Tunable potoluminescence of monolayer MoS_2 via chemical doping. *Nano Lett.* **2013**, *13*, 5944−5948.
(40) Kim, E.; Lee, Y.; Ko, C.; Park, Y.; Yeo, J.; Chen, Y.; Choe, H. S.; Allen, F. I.; Rho, J.; Tongay, S.; Wu, J.; Kim, K.; Grigoropoulos, C. P. Tuning the optical and electrical properties of MoS_2 by selective Ag photo-reduction. *Appl. Phys. Lett.* **2018**, *113*, 013105.
(41) Jung, C.; Yang, H. I.; Choi, W. Effect of ultraviolet-ozone treatment on MoS_2 monolayers: Comparison of chemical-vapor-deposited polycrystalline thin films and mechanically exfoliated single crystal flakes. *Nanoscale Res. Lett.* **2019**, *14*, 278.
(42) Kim, J. H.; Kim, T. H.; Lee, H.; Park, Y. R.; Choi, W.; Lee, C. J. Thickness-dependent electron mobility of single and few-layer MoS_2 thin-film transistors. *AIP Advances* **2016**, *6*, 065106.
(43) Li, H.; Wu, J.; Huang, X.; Lu, G.; Yang, J.; Lu, X.; Xiong, Q.; Zhang, H. Rapid and reliable thickness identification of two-dimensional nanosheets using optical microscopy. *ACS Nano* **2013**, *7*, 10344−10353.
(44) Tosun, M.; Fu, D.; Desai, S. B.; Ko, C.; Seuk Kang, J.; Lien, D.-H.; Najmzadeh, M.; Tongay, S.; Wu, J.; Javey, A. MoS_2 heterojunctions by thickness modulation. *Sci. Rep.* **2015**, *5*, 10990.
(45) Taniguchi, T.; Nurdiwijayanto, L.; Li, S.; Lim, H. E.; Miyata, Y.; Lu, X.; Ma, R.; Tang, D.-M.; Ueda, S.; Tsukagoshi, K.; Sasaki, T.; Osada, M. On/Off Boundary of Photocatalytic Activity between Single- and Bilayer MoS_2. *ACS Nano* **2020**, *14*, 6663−6672.

https://doi.org/10.1021/acsanm.3c00361
ACS Appl. Nano Mater. XXXX, XXX, XXX−XXX